HAL open science

One pot-synthesis of the fourth category of dinuclear molybdenum(VI) oxalate series: Structure and study of thermal and redox properties

Bougar Sarr, Abdou Mbaye, Cheikh A.K. Diop, Mamadou Sidibe, Frédéric Melin, Petra Hellwig, Francis Maury, François Senocq, Philippe Guionneau, Michel Giorgi, et al.

▶ **To cite this version:**

Bougar Sarr, Abdou Mbaye, Cheikh A.K. Diop, Mamadou Sidibe, Frédéric Melin, et al.. One pot-synthesis of the fourth category of dinuclear molybdenum(VI) oxalate series: Structure and study of thermal and redox properties. Inorganica Chimica Acta, 2019, 491, pp.84-92. ⟨10.1016/j.ica.2019.03.037⟩. ⟨hal-02098234⟩

HAL Id: hal-02098234

https://hal.science/hal-02098234v1

Submitted on 12 Apr 2019

HAL is a multi-disciplinary open access archive for the deposit and dissemination of scientific research documents, whether they are published or not. The documents may come from teaching and research institutions in France or abroad, or from public or private research centers.

L'archive ouverte pluridisciplinaire **HAL**, est destinée au dépôt et à la diffusion de documents scientifiques de niveau recherche, publiés ou non, émanant des établissements d'enseignement et de recherche français ou étrangers, des laboratoires publics ou privés.

Autorisation HAL

HAL Authorization

Open Archive Toulouse Archive Ouverte (OATAO)

OATAO is an open access repository that collects the work of Toulouse researchers and makes it freely available over the web where possible

This is an author's version published in: http://oatao.univ-toulouse.fr/23687

Official URL: https://doi.org/10.1016/j.ica.2019.03.037

To cite this version:

Sarr, Bougar and Mbaye, Abdou and Diop, Cheikh A.K. and Sidibe, Mamadou and Melin, Frédéric and Hellwig, Petra and Maury, Francis and Senocq, François and Guionneau, Philippe and Giorgi, Michel and Gautier, Romain *One pot-synthesis of the fourth category of dinuclear molybdenum(VI) oxalate series: Structure and study of thermal and redox properties.* (2019) Inorganica Chimica Acta, 491. 84-92. ISSN 0020-1693

Any correspondence concerning this service should be sent to the repository administrator: tech-oatao@listes-diff.inp-toulouse.fr

One pot-synthesis of the fourth category of dinuclear molybdenum(VI) oxalate series: Structure and study of thermal and redox properties

Bougar Sarr[a,*], Abdou Mbaye[b], Cheikh A.K. Diop[a], Mamadou Sidibe[a], Frederic Melin[c,*], Petra Hellwig[c], Francis Maury[d], Francois Senocq[d], Philippe Guionneau[e], Michel Giorgi[f], Romain Gautier[g]

[a] Laboratoire de Chimie Minérale et Analytique (LA.CHI.MIA), Département de Chimie, Faculté des Sciences et Techniques, Université Cheikh Anta Diop, Dakar, Senegal
[b] Laboratoire de Chimie et de Physique des Matériaux (LCPM), de l'Université Assane Seck de Ziguinchor (UASZ), BP: 523 Ziguinchor, Senegal
[c] Chimie de la Matière Complexe UMR 7140, Laboratoire de Bioélectrochimie et Spectroscopie, CNRS-Université de Strasbourg, 1 rue Blaise Pascal, 67070 Strasbourg, France
[d] CIRIMAT, Université de Toulouse, CNRS/INPT/UPS, 4 allée E. Monso, BP 44362, 31030 Toulouse cedex, France
[e] CNRS, Univ. Bordeaux, ICMCB, UMR 5026, 87 avenue du Dr A. Schweitzer, F-33608 Pessac, France
[f] Aix Marseille Univ, CNRS, Centrale Marseille, FSCM, Spectropole, Marseille, France
[g] Institut des Matériaux Jean Rouxel (IMN), Université de Nantes, CNRS, 2 rue de la Houssinière, BP 32229, 44322 Nantes Cedex 3, France

ABSTRACT

Three new dinuclear molybdenum(VI) oxalate $(Pr_2NH_2)_4 \cdot [Mo_2O_6(C_2O_4)_2]$ (1), $(^iPr_2NH_2)_4 \cdot [Mo_2O_6(C_2O_4)_2]$ (2) and $(HDabco)_4[Mo_2O_6(C_2O_4)_2] \cdot 2H_2O$ (3) compounds, have been prepared by one pot-synthesis at room temperature and characterized by single crystal X-ray diffraction and vibrational spectroscopies. Each compound contains the binuclear $[Mo_2O_6(C_2O_4)_2]^{4-}$ anion where each molybdenum is in an octahedral MoO_6 environment. In compound (3), the interconnection between $[Mo_2O_6(C_2O_4)_2]^{4-}$ anions, $[HDabco]^+$ cations and water molecules (H_2O) leads to an infinite inorganic-organic chain structure. Similarly, in compounds (1) and (2) the interactions between $[Mo_2O_6(C_2O_4)_2]^{4-}$ anions and respectively $[Pr_2NH_2]^+$ and $[^iPr_2NH_2]^+$ cations leads to an infinite inorganic-organic chain structure. A remarkable difference between the compounds is that in compounds (1) and (2) interactions between the chains involve only Van der Waals forces giving rise to layer-like structures, which also interact between them only by Van der Waals forces, whereas in compound (3) the chains interact also through hydrogen bonds giving a 3D supramolecular structure. The thermal properties of the compounds were investigated through thermogravimetric and differential thermal analyzes. The differences in the thermal decomposition of the compounds in the solid state are discussed in relation with their crystal structure. Cyclic voltammetry shows that the $[Mo_2O_6(C_2O_4)_2]^{4-}$ anion can be reduced in both aprotic solvent and water.

1. Introduction

Nowadays molybdenum chemistry remains one of the most exciting research focus areas. Various stable oxidation states ranging from −II to +VI and coordination numbers from 4 to 6 confer to molybdenum a very diversified chemistry and allow the preparation of compounds with very original properties. Among them, dialkylammonium dimolybdates and oxalate complexes of molybdenum (VI) like $M_2[Mo_2O_5(C_2O_4)_2(H_2O)_2]$ {M = NH_4, Na, K, Rb, Cs} exhibit photochemical and photochromic properties [1–5]. For $[Mo_2O_4(\mu2\text{-}O)\{HC(3,5\text{-}Me2pz)_3\}_2](BF_4)_2$ and $[Mo_2O_3(O_2)_2(\mu2\text{-}O)(H_2O)\{HC(3,5\text{-}Me_2pz)_3\}]$ catalytic performances have been observed while $[Mo_2O_4(O_2)_2L(H_2O)_2] \cdot H_2O$ {L = MBA (N-[1–morpholinobenzyl] acetamide), PBA (N-[1–piperidinobenzyl] acetamide)} and $Mo_2O_4(O_2)_2L(H_2O)_4$ {L = BTEH (Benzoic acid [1-(thiophen-2-yl) ethylidene] hydrazide), BTMH (benzoic acid [(thiophen-2-yl)methylene] hydrazide)} exhibit successfully antibacterial activities [6–8]. Since these pioneer studies [1–8] several dinuclear molybdenum(VI) oxalate and/or dinuclear molybdenum(VI) compounds have been isolated and characterized. All the dinuclear molybdenum(VI) oxalate complexes currently known can be classified into four distinct categories. The first category concerns the binuclear $[Mo_2O_3(C_2O_4)_4]^{4-}$ anion. Until now only one compound has been isolated and characterized, namely $(C_9H_{14}N)_2(C_8H_{12}N)_2[Mo_2O_3(C_2O_4)_4]$ [9]. The two metal ions are linked via a single (μ − oxo) bridge. The coordination sphere of each metal ion is completed by a terminal oxo ligand and two monochelating oxalates.

The dinuclear $[Mo_2O_4(C_2O_4)_2(L)_2]^{2-}$ anions where L is most often a neutral amine or a water molecule belong to the second category. Some typical examples include $Ba_2[Mo_2O_4(C_2O_4)_2(H_2O)_2] \cdot H_2O$, $(PyH)_2[Mo_2O_4(C_2O_4)_2Py_2]$, $(4\text{-Me-PyH})_3[Mo_2O_4(C_2O_4)_2(4\text{-}MePy)_2]Br$, $(4\text{-EtPyH})_2[Mo_2O_4(C_2O_4)_2(4\text{-EtPy})_2]$, $(PyH)_2[Mo_2O_4(C_2O_4)_2(3.5\text{-Lut})_2]$, $(PyH)_2[Mo_2O4(C_2O_4)_2(H_2O)_2]$ and $[(C_6H_5)_4P]_2[Mo_2O_4(C_2O_4)_2Py_2] \cdot H_2O$

* Corresponding authors.
E-mail addresses: bouks89@gmail.com (B. Sarr), fmelin@unistra.fr (F. Melin).

https://doi.org/10.1016/j.ica.2019.03.037

(Py = pyridine. 4-MePy = 4-methylpyridine. 4-EtPy = 4-ethylpyridine. 3.5-Lut = 3.5-lutidine) [10–12]. Each metal ion is coordinated by a terminal oxo ligand, a monochelating oxalate and a L ligand. In contrast to the previous category, the two metal ions are linked via a di-(μ oxo) bridge. The third category concerns the binuclear $[Mo_2O_5(C_2O_4)_2(H_2O)_2]^{2-}$ anions. Among many others we can mention $R_2[Mo_2O_5(C_2O_4)_2(H_2O)_2]$ (R = K, Rb, Cs, NH_4, PyH, γ-PicH, $(CH_3)_4N$ and Py = pyridinium, Pic = picolinium, …) [1–5,9,13,14]. In these oxomolybdate species each metal ion is coordinated by two terminal oxo ligands, a monochelating oxalate $(C_2O_4)^{2-}$ and water molecule (H_2O). The two metal ions are linked via a single (μ oxo) bridge. The fourth recently isolated and described category [15] concerns this binuclear $[Mo_2O_6(C_2O_4)_2]^{4-}$ anion, where each molybdenum atom is coordinated by a monochelating oxalate, two terminal oxo ligands and linked via a di-(μ oxo) bridge. In this category only one compound is currently known: $[Co(en)_3]_4[Mo_2O_6(C_2O_4)_2]$ [15].

However, this field of investigation of oxalatomolybdate compounds is still not fully explored.

Continuing our research on polyoxometalates as organic-inorganic hybrid materials, and more specifically on oxomolybdate complexes [16], we have isolated in the present paper three molybdenum oxalate anionic species with three different ammonium counter cations, dipropylamine, diisopropylamine and Dabco (1,4-diazabicyclo[2.2.2]octane), respectively. These binuclear species, namely $(Pr_2NH_2)_4{\cdot}[Mo_2O_6(C_2O_4)_2]$ (1), $(^iPr_2NH_2)_4{\cdot}[Mo_2O_6(C_2O_4)_2]$ (2) and $(HDabco)_4[Mo_2O_6(C_2O_4)_2]{\cdot}H_2O$ (3) were both obtained from the same reagents (ammonium heptamolybdate tetrahydrate and oxalic acid) and using a similar simple procedure (one pot-synthesis in aqueous phase). All three compounds contain the same binuclear $[Mo_2O_6(C_2O_4)_2]^{4-}$ anion. Their structures have been determined by X-ray diffraction and confirmed by infrared and Raman spectroscopic studies. Thermal and redox properties of complexes were also investigated by thermogravimetric and/or differential thermal analysis and cyclic voltammetry.

2. Experimental section

2.1. Materials

Oxalic acid (100%), dipropylamine (98%), diisopropylamine (99%), Dabco (98%) and ammonium heptamolybdate tetrahydrate (100%) were purchased from Sigma-Aldrich and used without further purification. Methanol and distilled water were used as solvent.

2.2. Synthesis

$(Pr_2NH_2)_4{\cdot}[Mo_2O_6(C_2O_4)_2]$ (1): oxalic acid (1.00 g, 11.1 mmol), dipropylamine (2.24 g, 22.1 mmol) and ammonium heptamolybdate tetrahydrate (1.06 g, 0.9 mmol) were dissolved in water (60 ml) at room temperature. The solution was then stirred for one hour and evaporated in the oven at 60 °C to yield a whitish precipitate. The purification by recrystallization of the precipitate in methanol readily leads after 2-week slow evaporation at room temperature to pretty white crystals of 1 (60% yield).

$(iPr_2NH_2)_4{\cdot}[Mo_2O_6(C_2O_4)_2]$ (2): similarly to (1), oxalic acid (1.00 g, 11.1 mmol), diisopropylamine (2.24 g, 22.1 mmol) and ammonium heptamolybdate tetrahydrate (1.06 g, 0.9 mmol) were dissolved in water (60 ml). The solution was then stirred for one hour and evaporated in the oven at 60 °C to yield white crystals of 2 after four days (54% yield).

$(HDabco)4{\cdot}[Mo_2O_6(C_2O_4)_2]{\cdot}H_2O$ (3): this compound was obtained by direct reaction of oxalic acid (1.00 g, 11.1 mmol), Dabco (2.50 g, 22.1 mmol) and ammonium heptamolybdate tetrahydrate (1.06 g, 0.9 mmol) after dissolution in water (60 ml) at room temperature. The solution was then stirred for one hour and evaporated in the oven at 60 °C to yield a whitish precipitate. The purification of this precipitate carried out by recrystallization in methanol leads after 2-week slow evaporation at room temperature to pretty white crystals of 3 (72% yield).

2.3. Elemental analyses (C, H, N) measurements

Elemental CHN analyses were performed using a PERKIN ELMER 2400 serie II analyzer. Two experimental analyses were made for each compound and the reproducibility is very good as shown by the low absolute uncertainties. The theoretical and experimental values found for the three compounds are given hereafter. Compound (1): Theoretical: C: 38.5%, H: 7.3%, N: 6.4%; Experimental: C: 38.84 ± 0.10%, H 8.61 ± 0.04%, N: 6.49 ± 0.02%. Compound (2): Theoretical: C: 38.5%, H: 7.3%, N: 6.4%; Experimental: C: 38.00 ± 0.10%, H: 8.32 ± 0.11%; N: 6.85, 6.79 ± 0.06%. Compound (3): Theoretical: C: 35.30%, H: 5.92%, N: 11.76%; Experimental: C: 32.52 ± 0.07%; H: 6.75 ± 0.06%; N: 10.75 ± 0.01%.

2.4. Powder X-ray diffraction (PXRD) measurements

Powder X-ray diffraction (PXRD) patterns were measured at room temperature with a Bruker AXS D8 diffractometer using Cu-Kα radiation (λ = 1.5418 Å).

2.5. Structure determination

Suitable crystals for compounds $(Pr_2NH_2)_4{\cdot}[Mo_2O_6(C_2O_4)_2]$ (1), $(^iPr_2NH_2)_4{\cdot}[Mo_2O_6(C_2O_4)_2]$ (2) and $(HDabco)_4{\cdot}[Mo_2O_6(C_2O_4)_2]{\cdot}H_2O$ (3) were measured on a Rigaku Oxford Diffraction SuperNova diffractometer at 293 K at the MoKα radiation (λ = 0.71073 Å). Data collection reduction and multiscan ABSPACK correction were performed with CrysAlisPro (Rigaku Oxford Diffraction). The structure was solved by Patterson method using ShelXT-2015 and refined with SHELXL-2015 [17,18]. Crystallographic Information files were compiled with Olex2.12 [19]. Crystallographic data are summarized in Table 1.

2.6. Spectroscopic measurements

The IR spectra were recorded with a Vertex 70 spectrometer from Bruker equipped with a Harrick diamond ATR cell, a globar source and a KBr beamsplitter. 256 scans with 4 cm^{-1} resolution were averaged. The final spectra were corrected from the atmospheric contributions of H_2O and CO_2 gases. The Raman spectra were obtained with an Invia Raman Microscope from Renishaw operating at $\lambda = 514$ nm. Five spectra obtained with 10 s irradiation time and 25 mW laser power were averaged.

2.7. TGA measurements

Thermogravimetric analysis (TGA) measurement was carried out with a Setaram Sensys Evo under Argon flow, from room temperature to 1000 °C with a heating rate of 10 °C min^{-1}. These conditions allow to study only the thermal stability under inert gas and not the degradation by reaction at high temperature in an oxidizing medium (in air for example), which would be more complex. The test portion of each product was between 14 and 24 mg. The return to ambient temperature (25 °C) from the 1000 °C at the end of the analysis was made always under Ar flow with a negative temperature ramp of −33 °C min^{-1}.

2.8. Cyclic voltammetry measurements

The cyclic voltammetry measurements were carried out either in DMSO with 0.1 M nBu_4PF_6 or in H_2O with 0.1 M KCl as supporting electrolyte with a conventional three electrodes cell connected to a

Table 1
Crystallographic data of compounds 1, 2 and 3.

Compound	(1)	(2)	(3)
Formula weight (g mol^{-1})	872.71	872.71	952.68
Crystal system	Orthorhombic	Triclinic	Monoclinic
Space group	$Pca2_1$	$P-1$	$P2_1/c$
a (Å)	9.1509 (1)	8.5134 (1)	10.96383 (15)
b (Å)	21.9124 (3)	9.6363 (1)	17.9763 (2)
c (Å)	21.6434 (3)	12.4286 (6)	9.75418 (14)
α (°)	90	83.136 (1)	90
β (°)	90	84.244 (1)	100.0550 (13)
γ (°)	90	84.999 (1)	90
V (Å^3)	4339.90 (10)	1004.28 (5)	1892.92 (5)
Z	4	2	4
Temperature (K)	293	298	293
μ (mm^{-1})	0.64	0.69	0.74
Crystal size (mm^3)	0.34 × 0.32 × 0.16	0.30 × 0.30 × 0.16	0.34 × 0.24 × 0.14
R1[I = 2σ(I)]	0.035	0.021	0.025
w*R*2[I = 2σ(I)]	0.095	0.060	0.060
Radiation	Mo*Kα* radiation (λ = 0.71073 Å)	Mo*Kα* radiation, λ = 0.71073 Å	Mo*Kα* radiation (λ = 0.71073 Å)
2Θ range for data collection v	3.4–27.5	2.8–30.1	3.9–28.1
hkl range	$-11 \le \mathbf{h} \le 11$; $-28 \le \mathbf{k} \le 28$; $-27 \le \mathbf{l} \le 27$	$-11 \le \mathbf{h} \le 11$; $-13 \le \mathbf{k} \le 13$; $-17 \le \mathbf{l} \le 17$	$-14 \le \mathbf{h} \le 14$ $-23 \le \mathbf{k} \le 24$; $-12 \le \mathbf{l} \le 12$
Reflections collected	92,083	5831	55,943
Independent reflections	9333	233	4491
Goodness-of-fit on F^2	1.05	1.10	1.05
Largest diff. peak/hole (e A^{-3})	0.50/−0.32	0.34/−0.76	0.30/−0.48

Princeton Applied Research VERSASTAT 4 potentiostat. In H_2O, the pH of the solution was adjusted by adding small aliquots of 1 M hydrochloric acid or sodium hydroxide solutions. A 3 mm diameter glassy carbon disk was used as working electrode and a platinum wire as counter electrode. A silver chloride electrode (3 M KCl) was used as reference electrode in aqueous solution and a platinum wire as pseudo reference electrode in DMSO. In the latter case, ferrocene was added at the end of the experiment and used as internal standard. The solutions were degassed with argon for 20 min prior to the measurements.

3. Results and discussion

3.1. Elemental analysis using CHN

For the compounds (1) and (2), the experimental data are in very good agreement with the expected composition according to the empirical formula determined by the crystallographic structure. The difference between the theoretical and experimental values for the compound (3) reveals the presence of impurities. For all three compounds, the presence of the oxomolybdic moieties (Mo_2O_6) results from fragmentation reactions of ammonium heptamolybdate tetrahydrate (AHM) used as starting material. Hence the residual presence of 7.8% percent of AHM as an impurity in the compound (3) would lower the calculated relative contents of C (35.30% for the pure product) to reach a satisfactory agreement with the experimental values (*ca.* 32.5% in the presence of AHM impurity).

3.2. Powder X-ray diffraction (PXRD)

The purity of compounds was also monitored by powder X-ray diffraction (PXRD). The similarity of the experimental and calculated PXRD patterns of compounds (see Fig. SI1, in Supporting information) indicated that synthesized compounds match with the simulated one respectively, except for some intensity difference. The intensity differences can be owed to the different orientation of the crystals in the powder samples. The impurities revealed by the CHN analysis for compound 3 are confirmed by the powder X-ray diffraction (PXRD) showing two additional peaks on the experimental XRD powder patterns of this compound (3). These two peaks at 2θ (°) = 32 and 40 can be attributed to the presence of ammonium heptamolybdate tetrahydrate in compound (3) as impurities [20].

3.3. Crystal structures description

The three title compounds consist of $[Mo_2O_6(C_2O_4)_2]^{4-}$ dinuclear complex anions (Fig. 1) stabilized by either $[Pr_2NH_2]^+$, $[^iPr_2NH_2]^+$ or $[HDabco]^+$ cations. The compound (1) crystallizes in an orthorhombic $Pca2_1$ space group system. Its asymmetric unit consists of one $[Mo_2O_6(C_2O_4)_2]^{4-}$ and four $[Pr_2NH_2]^+$ cations. The compound (2) crystallizes in a triclinic $P-1$ space group system. Its asymmetric unit consists of half $[Mo_2O_6(C_2O_4)_2]^{4-}$ and two $[Pr_2NH_2]^+$ cations. The compound (3) crystallizes in a monoclinic $P2_1/c$ space group system. Its asymmetric unit consists of half $[Mo_2O_6(C_2O_4)_2]^{4-}$, one lattice water molecule (H_2O) and two $[HDabco]^+$ cations. In all three compounds, each molybdenum is in its highest degree of oxidation (Mo^{VI}). This oxidation state exhibits a much richer chemistry than any of other oxidation states of molybdenum, namely −II, 0, +II, +III, +IV, V and +VI [21]. The metal displays here a marked tendency to dimerize through two oxygen bridges to form the $\{Mo_2O_6\}$ fragment. The coordination sphere of each molybdenum is completed by a bidentate oxalate (Fig. 1). Each oxalate ligand is linked to the molybdenum center via two oxygen atoms, all being in cis to the terminal oxo ligands. For all compounds, the two oxygen bridges are not quite symmetrical; the two Mo—O distances are at 2.198 (4) Å**,** 1.783 (3) Å, 1.790 (3) Å, 2.201 (4) Å for the (1); 1.8409 (9) Å, 2.1631 (8) Å for the (2) and 1.8229 (11)

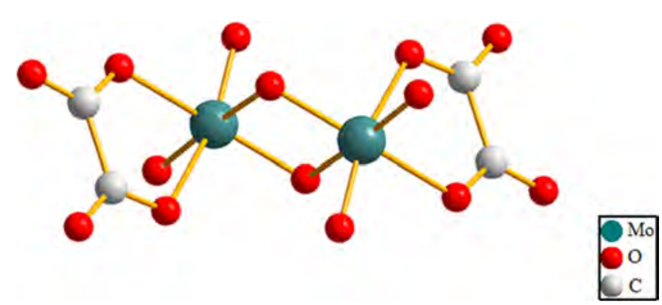

Fig. 1. Dinuclear anion $[Mo_2O_6(C_2O_4)_2]^{4-}$ in compounds 1–3.

Table 2
Selected bond lengths (Å) and bond angles (°) in compounds 1, 2 and 3.

Compound (1)		Compound (2)	Compound (3)
Mo1—Mo2 3.1191 (5)	O4—Mo1—Mo2 81.79 (11)	Mo1—Mo1^{i} 3.1464 (2)	Mo1—Mo1^{i} 3.1854 (3)
Mo1—O1 1.694 (4)	O7—Mo1—Mo2 34.09 (9)	Mo1—O2 1.6981 (10)	Mo1—O1 2.2337 (13)
Mo1—O2 1.727 (5)	O7—Mo1—O4 74.84 (14)	Mo1—O7 1.7364 (10)	Mo1—O2 2.1362 (12)
Mo1—O3 2.172 (3)	O8—Mo1—Mo2 43.52 (12)	Mo1—O1 1.8409 (9)	Mo1—O5^{i} 2.2370 (11)
Mo1—O4 2.271 (3)	O8—Mo1—O3 153.77 (17)	Mo1—O4 2.1312 (9)	Mo1—O5 1.8229 (11)
Mo1—O7 2.198 (4)	O8—Mo1—O4 93.78 (15)	Mo1—O1^{i} 2.1631 (8)	Mo1—O6 1.7033 (14)
Mo1—O8 1.783 (3)	O8—Mo1—O7 77.60 (15)	Mo1—O3 2.2898 (9)	Mo1—O26 1.7193 (14)
Mo2—O7 1.790 (3)	O7—Mo2—Mo1 43.48 (12)	O3—C1 1.2513 (15)	O1—C1 1.257 (2)
Mo2—O8 2.201 (4)	O7—Mo2—O8 77.40 (15)	O4—C2 1.2785 (16)	O2—C2 1.276 (2)
Mo2—O9 1.730 (3)	O7—Mo2—O11 152.61 (17)	O5—C1 1.2455 (16)	O3—C2 1.224 (2)
Mo2—O10 1.725 (5)	O7—Mo2—O12 87.99 (14)	O6—C2 1.2248 (16)	O4—C1 1.237 (2)
Mo2—O11 2.144 (3)	O8—Mo2—Mo1 33.92 (9)	O1—Mo1^{i} 2.1631 (8)	O5—Mo1^{i} 2.2370 (11)
Mo2—O12 2.227 (3)	O8—Mo2—O12 77.76 (15)	O2—Mo1—O7 103.41 (6)	O1—Mo1—Mo1^{i} 80.89 (4)
O3—C2 1.262 (6)	O9—Mo2—Mo1 99.71 (17)		O1—Mo1—O5^{i} 77.80 (5)
O4—C1 1.238 (6)	O9—Mo2—O7 107.35 (18)	O2—Mo1—O1 105.54 (5)	O2—Mo1—Mo1^{i} 111.22(4)
O5—C1 1.241 (6)	O9—Mo2—O8 89.5 (2)	O7—Mo1—O1 99.96 (5)	O2—Mo1—O1 73.07 (4)
O6—C2 1.227 (6)	O9—Mo2—O11 87.11 (16)	O2—Mo1—O4 89.70 (5)	O2—Mo1—O5^{i} 78.20 (4)
O11—C3 1.271 (6)	O9—Mo2—O12 157.62 (16)	O7—Mo1—O4 96.68 (5)	O5—Mo1—Mo1^{i} 43.20 (4)
O12—C4 1.246 (6)	O10—Mo2—Mo1 144.65 (18)	O1—Mo1—O4 154.01 (4)	O5^{i}—Mo1—Mo1^{i} 33.91 (3)
O13—C4 1.234 (6)	O10—Mo2—O7 103.8 (2)	O2—Mo1—O1^{i} 95.04 (5)	O5—Mo1—O1 89.00 (5)
O14—C3 1.223 (6)	O10—Mo2—O8 164.82 (19)	O7—Mo1—O1^{i} 161.44 (5)	O5—Mo1—O2 152.04 (5)
	O10—Mo2—O9 104.3 (2)	O1—Mo1—O1^{i} 76.70 (4)	O5—Mo1—O5^{i} 77.11 (5)
O1—Mo1—Mo2 103.8 (2)	O10—Mo2—O11 94.6 (2)	O4—Mo1—O1^{i} 81.16 (4)	O6—Mo1—Mo1^{i} 99.12 (5)
O1—Mo1—O2 103.3 (3)	O10—Mo2—O12 87.1 (2)	O2—Mo1—O3 161.49 (5)	O6—Mo1—O1 160.14 (6)
O1—Mo1—O3 85.80 (17)	O11—Mo2—Mo1 112.33 (12)	O7—Mo1—O3 83.86 (5)	O6—Mo1—O2 88.67 (6)
O1—Mo1—O4 157.04 (17)	O11—Mo2—O8 79.64 (15)	O1—Mo1—O3 89.63 (4)	O6—Mo1—O5 104.69 (6)
O1—Mo1—O7 97.1 (2)	O11—Mo2—O12 72.63 (12)	O4—Mo1—O3 72.41 (3)	O6—Mo1—O5^{i} 91.09 (6)
O1—Mo1—O8 105.61 (19)	O12—Mo2—Mo1 80.01 (12)	O1^{i}—Mo1—O3 77.91 (4)	O6—Mo1—O26 103.28 (8)
O2—Mo1—Mo2 142.1 (2)		O2—Mo1—Mo1^{i} 102.54 (4)	O26—Mo1—Mo1^{i} 145.46 (5)
O2—Mo1—O3 96.6 (2)		O7—Mo1—Mo1^{i} 138.84 (4)	O26—Mo1—O1 86.53 (7)
O2—Mo1—O4 83.57 (19)		O1—Mo1—Mo1^{i} 41.99 (3)	O26—Mo1—O2 95.36 (6)
O2—Mo1—O7 158.39 (19)		O4—Mo1—Mo1^{i} 114.85 (3)	O26—Mo1—O5 104.99 (6)
O2—Mo1—O8 103.4 (2)		O1^{i}—Mo1—Mo1^{i} 34.71 (2)	O26—Mo1—O5^{i} 164.19 (6)
O3—Mo1—Mo2 111.33 (11)		O3—Mo1—Mo1^{i} 81.50 (2)	
O3—Mo1—O4 71.55 (12)			
O3—Mo1—O7 77.59 (14)			

Symmetry transformations used to generate equivalent atoms: compound (1): (i) x − 1/2, −y + 2, z; (ii) −x + 3/2, y, z + 1/2; (iii) x − 1/2, −y + 1, z; compound (2): (i) –x, −y, −z + 1 and compound (3): (i) –*x*, −*y* + 1, −*z* + 1.

Å, 2.2370 (11) Å for the (3) (Table 2). The binuclear unit consists of two molybdenum centers in distorted octahedral environments. The two metal ions are linked by double bridge (μ-oxo). In the binuclear anion, the interaction between two metal ions is at Mo–Mo distance equal to 3.1191 (5) Å, 3.1464 (2) Å and 3.1854 (3) Å respectively for the compounds (1), (2) and (3).

The $[Mo_2O_6(C_2O_4)_2]^{4-}$ anions thus consist of two MoO_6 octahedra contiguous on one side. The variation of the Mo—O bond lengths [in the 1.694 (4)–2.271 (3) Å range for (1), in the 1.6981 (10)–2.2898 (9) Å range for (2) and in the 1.7033 (14)–2.2370 (11) Å range for (3)] as well as that of the O—Mo—O angles [in the 71.55 (12)–158.39 (19) ° range for (1), in the 72.41 (3)–161.49 (5)° range for (2) and in the 73.07 (4)–164.19 (6)° range for (3)] confirms that the octahedra are irregular (Table 2). Overall, the Mo—O lengths and O—Mo—O angles found here are consistent with $[Mo_2O_5(C_2O_4)_2(H_2O)_2]^{2-}$ dinuclear complexes anions previously reported [22–24].

Mo—O bond lengths for shared oxygen [Mo1—O3 = 2.172 (3) Å, Mo1—O4 = 2.271 (3) Å, Mo2—O7 = 1.790 (3) Å, Mo2—O8 = 2.201 (4) Å, Mo2—O11 = 2.144 (3) Å, Mo2—O12 = 2.227 (3) Å for the (1), Mo1—O1^{i} = 2.1631 (8) Å, Mo1—O4 = 2.1312 (9) Å, Mo1—O3 = 2.2898 (9) Å for the (2) and Mo1—O1 = 2.2337 (13) Å, Mo1—O2 = 2.1362 (12) Å, Mo1—O5i = 2.2370 (11) Å, Mo1—O5 = 1.8229 (11) Å for the (3)] are significantly higher than the Mo—O bonds for terminal oxygen Ot [Mo1—O1 = 1.694 (4) Å, Mo1—O2 = 1.727 (5) Å, Mo2—O9 = 1.730 (3) Å, Mo2—O10 = 1.725 (5) Å for the (1), Mo1—O1 = 1.8409 (9) Å, Mo1—O2 = 1.6981 (10) Å, Mo1—O7 = 1.7364 (10) Å for the (2) and Mo1—O6 = 1.7033 (14) Å, Mo1—O26 = 1.7193 (14) Å for the (3)]. This suggests, for all compounds, that Mo—Ot are double bonds and Mo-(μ-oxo) single bonds. Furthermore the Mo—Ot bond lengths are in good agreement with Mo═O double bonds reported in the literature [25,26]. In addition, depending on the oxygen atoms involved in the coordination of molybdenum, the oxalate C—O bond lengths vary slightly.

For each compound, the oxalate C—O bond lengths for oxygen involved in the coordination of Mo(VI) [O3—C2 = 1.262 (6) Å, O4—C1 = 1.238 (6) Å, O11—C3 = 1.271 (6) Å, O12—C4 = 1.246 (6) Å for the (1), O3—C1 = 1.2513 (15) Å, O4—C2 = 1.2785 (16) Å for the (2) and O2—C2 = 1.276 (2) Å, O1—C1 = 1.257 (2) Å for the (3)] are slightly higher than the C—O bonds, for uninvolved oxygen [O5—C1 = 1.241 (6) Å, O6—C2 = 1.227 (6) Å, O13—C4 = 1.234 (6) Å, O14—C3 = 1.223 (6) Å for the (1), O5—C1 = 1.2455 (16) Å, O6—C2 = 1.2248 (16) Å for the (2) and O3—C2 = 1.224 (2) Å, O4—C1 = 1.237 (2) Å for the (3)]. This may be due to the same disturbance phenomenon.

In compound (3), the anion is stabilized by four $[HDabco]^{+}$ cations through simple N—H···O and bifurcated N—H···(O, O) hydrogen bonds, respectively involving O5 bridging oxygen and (O3, O4) oxygen atoms. This leads to the neutral entity $(HDabco)_4[Mo_2O_6(C_2O_4)_2]$. Each $(HDabco)_4[Mo_2O_6(C_2O_4)_2]$ entity connects to its neighbor through lattice water molecules. The interactions are via the O26 of MoO_3 and O3 of oxalate through two links of hydrogen bonds of types O26···H—O7—H···O3. This leads to the infinite chain shown in Fig. 2c. We note that the same oxygen atom O3 involved in the hydrogen-bifurcated bond N—H···(O3, O4) is also involved in the single bond O7—H···O3, while O6 oxygen atoms remain “free”. The overall structure of the compound consists of infinite chains not connected but interacting with each other by Van der Waals forces (see Fig. SI2c, in Supporting information). The electronic correlation effects of Van der

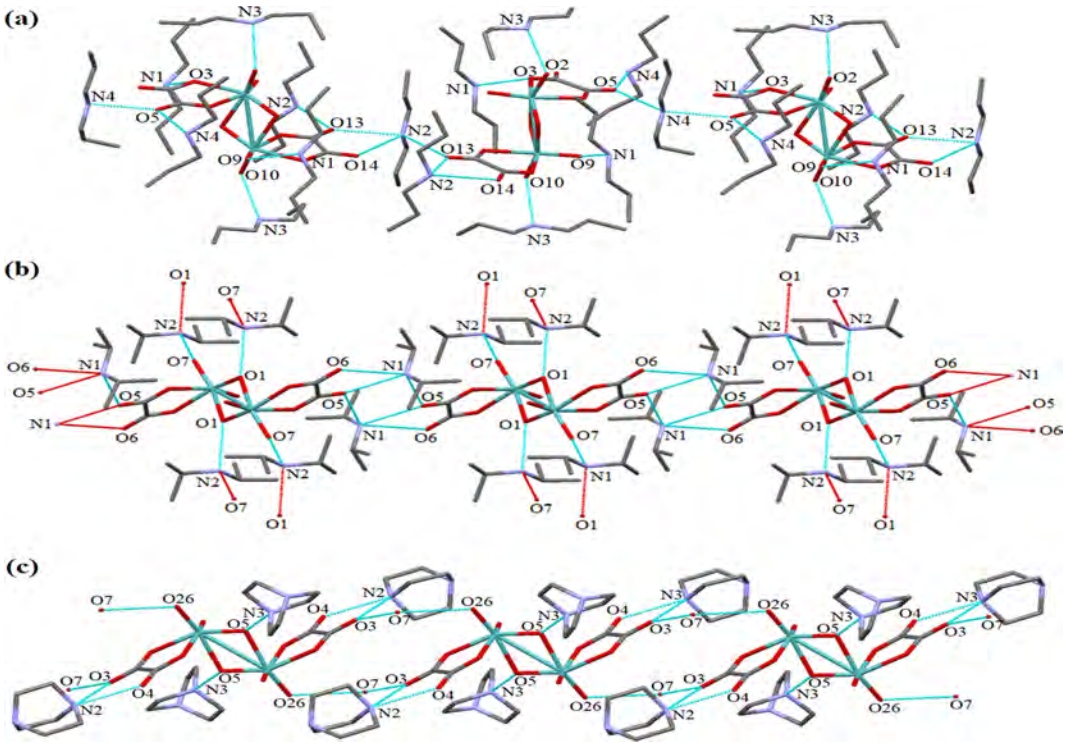

Fig. 2. Infinite chains in compounds 1 (a), 2 (b) and 3 (c). Hydrogen atoms are omitted for clarity.

Waals forces are purely no localized and in none case a local or semi-local approximation will not be able to account for it. However, we can note that along the b-axis the metal-metal (Mo⋯Mo) distances for adjacent chains at short range are in the order of 8.6 Å and those at long range about 11.9 Å. In compound (3), $[HDabco]^+$ cations cannot act as bridges between two different anions. This, partly because of the impossibility of direct interaction between an oxygen of the anion and the non-protonated nitrogen atom. In addition, the steric strain of a tertiary ammonium group prevents the hydrogen atom to get involved in a bifurcated hydrogen bond bridging two different anions. As a consequence, the presence of water molecules is required to ensure the anion-anion connections in compound (3).

In contrast, the anion-anion interactions in compounds (1) and (2) do not require the presence of water molecules because they can be ensured respectively by two protons of the dipropylammonium and diisopropylammonium cations. Thus, in compound (1) each binuclear entity $[Mo_2O_6(C_2O_4)_2]^{4-}$ interacts with eight dipropylammonium cations through bifurcated N—H⋯(O, O) [N1—H⋯(O3, O6), N2—H⋯(O13, O14), N4—H⋯(O5, O6)] and simples N—H⋯O [N1—H⋯O9, N2—H⋯O13, N3—H⋯O2, N3—H⋯O10, N2—H⋯O2, N4—H⋯O5] hydrogen bonds, involving oxo ligands (O^{2-}) or oxygen oxalates.

We can note that except O1, all the oxo (O^{2-}) ligands within the binuclear anion are involved in hydrogen bonds.

The fact that the oxygen atom O1 is not involved in hydrogen bonds is manifested by the short length Mo1—O1 (1.694 (4) Å) as compared to other Mo—O lengths of the complex anion [Mo1—O3 = 2.172 (3), Mo1—O4 = 2,271 (3), Mo2—O7 = 1.790 (3) Å, Mo2—O8 = 2.201 (4) Å, Mo2—O11 = 2.144 (3) Å, Mo2—O12 = 2.227 (3) Å, Mo1—O1 = 1.694 (4) Å, Mo1—O2 = 1.727 (5) Å, Mo2—O9 = 1.730 (3) Å, Mo2—O10 = 1.725 (5) Å].

Thus, each binuclear anion $[Mo_2O_6(C_2O_4)_2]^{4-}$ bound to four dipropylammonium stabilizing cations connects to two neighbors via four others to lead to an infinite chain shown in Fig. 2a.

The global structure is a stack of infinite chains interacting through hydrogen bonds N—H⋯O, N—H⋯(O, O) involving cations and anions giving rise to a 3D network (see Fig. SI2a, in Supporting information). In this structure, by occupying their crystallographic sites, the dipropylammonium cations are arranged in such a way as to leave free tunnels into which $[Mo_2O_6(C_2O_4)_2]^{4-}$ zigzag ribbons are inserted. Moreover, in compound (2), the anion laterally connected to four $[^iPr_2NH_2]^+$ links to two neighbors via four cations. These interactions involve simple N—H⋯O and bifurcated N—H⋯(O, O) hydrogen bonds, involving respectively O1, O7 or O5 and (O5, O6). This leads to an infinite chain (Fig. 2b). In addition, these infinite chains interact through simple hydrogen bonds, N2—H⋯O1 and N2—H⋯O7, leading to an infinite layer structure (see Fig. SI2b, in Supporting information). As in compound (1), only van der Waals interactions are observed between the layers. The absence of disturbance of oxygen atom O2 via interactions of hydrogen bonding type is also manifested by the short length Mo—O2 (1.6981 (10) Å) as compared to its counterparts [Mo1—O7 = 1.7364 (10) Å, Mo1—O1 = 1.8409 (9) Å, Mo1—O4 = 2.1312 (9) Å, Mo1—O1^i = 2.1631 (8) Å, Mo1—O3 = 2.2898 (9) Å, O1—Mo^i = 2.1631 (8) Å].

3.4. IR spectra

As expected from their common core structure, the three compounds exhibit a similar infrared spectral signature (see Fig. SI3, in Supporting information). We focus here on the attribution of the most characteristic bands. In the high frequency region of the spectra, the signals between 3000 and 2400 cm^{-1} can be assigned to the (N—H) and (C—H) stretching vibrations of the secondary or tertiary ammonium groups [27–29]. Compound 3 also exhibits two additional bands at 3437 and 3488 cm^{-1} which can be attributed to the (O—H) stretching vibration of the lattice water molecules. The oxalate ligands exhibit three sets of characteristic bands which reflect their binding mode [30]. Compound (1) exhibits three distinct bands at 1682, 1652 and 1626 cm^{-1}, whereas compounds (2) and (3) only two at 1653, 1625 and 1666, 1633 cm^{-1} respectively. This seems consistent with the higher variation of C—O bond lengths observed in compound (1). The $_s$(O—C—O) stretching vibrations contribute in the 1450–1280 cm^{-1} range. Each complex exhibit two main bands, at 1337–1347 cm^{-1} and 1280–1290 cm^{-1}. The δ(O—C—O) bending vibrations probably contribute to the band observed at 791 cm^{-1} for compound (1) and 785 cm^{-1} for compounds (2) et (3). The position of the oxalate bands here are consistent with those reported before for analogous compounds containing terminal bidentate oxalates [9,10,24].

The bands in the 1000–850 cm^{-1} range can be attributed to the ν(Mo═Ot) stretching vibrations. Compound (1) exhibits two large splitted bands centered at 907 and 851 cm^{-1}, whereas compound (2) and (3) shows two narrower bands centered at 931/858 and 918/871 cm^{-1} respectively. This again reflects the higher dissymmetry of the {Mo_2O_6} core in compound (1). The intense band observed in the 710–750 cm^{-1} range for the three compounds can be attributed to the ν(Mo—O—Mo) stretching vibrations [9,31].

3.5. Raman spectra

Raman spectroscopy is an appropriate and highly efficient tool for the identification of oxomolybdenum species [32–38]. The Raman absorption bands in the 1000–600 cm^{-1} region (See Fig. SI4, in Supporting information) indicate the presence of oxomolybdic fragments. The (Mo═Ot) stretching modes are observed at 921, 894 and 858 cm^{-1} for compound (1), 933 and 863 cm^{-1} for compound (2) and 921 and 873 for compound (3) [36–38]. The positions of these bands are consistent with their counterparts in the IR spectra. At lower wavenumbers the bands between 800 and 650 cm^{-1} are typical for the vibrations of double-bridged Mo—O—Mo modes [36–38]. At higher frequency, the C—O stretching vibrations of the oxalate ligands (1450–1430 cm^{-1} for the symmetric modes and 1660–1690 for the antisymmetric modes) and the C—H stretching vibrations of the ammonium cations (3000–2800 cm^{-1}) range contribute [39].

3.6. Thermal analyses

The thermal properties of the compounds were investigated by thermogravimetric analysis (TGA). Between 0 and 1000 °C under inert atmosphere (Ar), the TGA curve of compound (1) (see blue trace in Fig. 3) indicates a total mass loss of the order of 92% in several steps reflecting a continuous degradation mechanism. The thermal stability of the compound was observed up to 140 °C. A first loss of mass of the order of 20% of the total mass occurring in 140–210 °C range corresponds to the departure of the 2[C_2O_4]. This is done in 2 endothermic peaks which overlap around 180 °C. The second mass loss of the order of 46% is carried out in 210–350 °C range. This loss of mass due to the cations is done in 4 stages which are distinguished on the DTA curve: 3 peaks grouped at 225, 240 and 250 °C, and a fourth at 350 °C (Fig. 4). The third loss of mass of the order of 10% occurs slowly in 350–780 °C

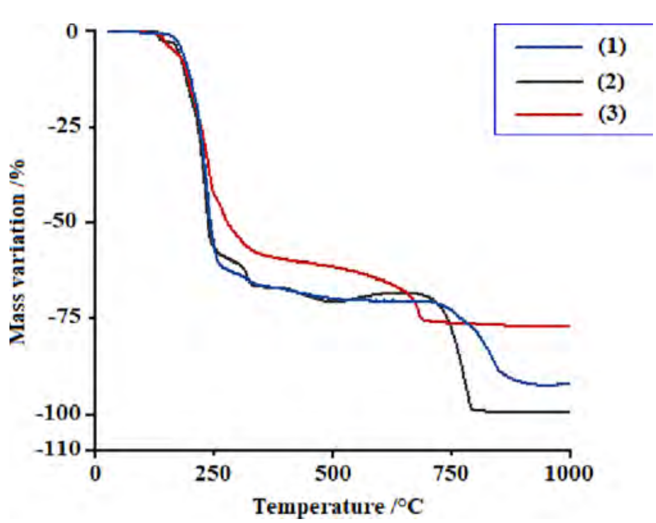

Fig. 3. TGA diagrams of compounds (1), (2) and (3).

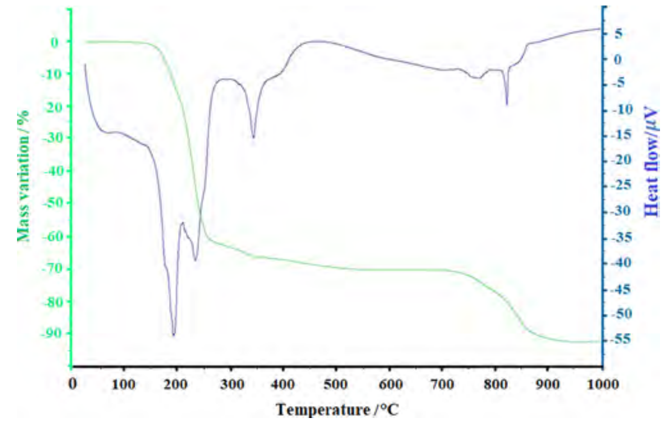

Fig. 4. TGA (green curve) and DTA (blue curve) diagrams of compound (1). (For interpretation of the references to colour in this figure legend, the reader is referred to the web version of this article.)

range. The process is at least two steps based on the slope changes of the TGA curve. This loss is assigned to the progressive decomposition of Mo_2O_6 entities into volatile MoO_3 molecules with the departure of x moles of MoO_3 which sublimes from the solid residue [40]. The 10% loss of mass could then correspond to approximately 0.67MoO_3 moles. So we would have the decomposition reaction:

$$Mo_2O_6(s) \rightarrow (2\text{–}0.67 = 1.33)MoO_3(s) + 0.67\ MoO_3(g)$$

The MoO_3 melting corresponds to the large endothermic peak at around 770 °C because in the environment of the crucible of the TGA analyzer, it must be considered that it has impurities with this MoO_3 phase (for example the other residues resulting from the decomposition in progress).

Since the presence of impurities in a solid lowers its melting point it is normal for it to drop from 795 (pure) to about 770 °C in our case. It follows that the very fine endothermic peak at 825 °C would correspond to the vaporization of a mole of MoO_3. This loss of one mole of MoO_3 occurs from 780 to 920 °C and is from the liquid phase (since MoO_3 is melted) which is a fairly fast process, in any case faster than the sublimation loss from a solid. After as indicated below, there would remain the solid residue of approximately 0.33 MoO_x corresponding to a mass of about 8% of non-volatile oxides as MoO_2 and mixed-valence oxides. The TGA diagram of compound (2) (black trace in Fig. 3) is quite similar to that of compound (1). One difference is a very sharp loss of mass of about 2% at 130 °C which is not representative of the loss of water from the crystal lattice. It could be due to the loss of contamination water (adsorbed) since this compound is the only one of the series that has not been recrystallized from methanol. Thereafter the loss of the 2 C_2O_4 (exp. 19 wt%; cal. 20 wt%) occurs in the 160–210 °C range, then the 4 $^{i}Pr_2NH_2$ (exp. 45 wt%; cal. 46 wt%) in the temperature range 210–340 °C. The thermal decomposition of the Mo-based entity is substantially different than in the compound (1) since it starts at the same temperature (340 °C) but ends at 800 °C (instead of 920 °C) without leaving a solid residue: experimental loss 36 wt% (instead of 26 wt% for compound (1)); calculated 33 wt% for Mo_2O_6. This decomposition occurs in two steps, 340–690 °C (4.0 wt%) and a second one (690–800 °C) largely dominant (33 wt%).

For compound (3) (red trace in Fig. 3), the curve indicates a total mass loss of the order of 78% in several steps reflecting also a continuous degradation mechanism of the compound. The water content in the crystal lattice was detected from mass loss of the order of 3% (3.8% calculated) is observed in the 125–160 range. This is a departure of a molecule of water (hydration water molecule). A second fast mass loss of the order of 13% (18.9% calculated) taking place in the 160–210 °C range corresponds to departure of the two ($C_2O_4^{2-}$) anions in the form of carbon dioxide (CO_2) but it is difficult to distinguish from the next

Table 3
Temperature range corresponding to the successive loss of the different entities constituting the three compounds.

Compound	Lost entities (experimental wt%)				Solid residue (wt%)
	H_2O	C_2O_4	Amine	Mo_2O_6	
(1)	N/A	140–210 (20.2)	210–350 (46.0)	350–780 (10.0) 780–920 (16.0)	8
(2)	130 (2.0)[a]	160–210 (19.0)	210–340 (45.0)	340–690 (4.0) 690–800 (32.0)	0
(3)	125–160 (3.0)	160–210 (13)	210–450 (45)	450–690 (15.0) 690–900 (2.0)	22

[a] Very sharp decrease which is not representative of the loss of water from the crystal lattice. This could be due to contamination water (adsorbed).

step (a slope change is visible at 210 °C). The third mass loss in the 210–450 °C range occurs in several steps and probably corresponds to departure of the 4 $[HDabco]^+$ cations. This overall loss is of the order of 45 wt% (48.2% calculated). The fourth loss of mass in the 450–900 °C range corresponds to the decomposition of the Mo_2O_6 entity with release of molybdenum trioxide and possibly oxygen. It occurs with a dominant step in the 450–690 °C (exp. 15%) assigned to the loss of one MoO_3 (cal. 15%) and a very slow loss in the 690–900 °C (only 2%) leaving a solid residue of 22% at 1000 °C corresponding likely to O_2 release and the formation of refractory molybdenum oxides as MoO_2 which is the most stable at high temperature [41]. Numerical data of the TGA analyses of the three compounds are reported in Table 3.

It allows a quick comparison of the thermal properties of all compounds. Oxalate ligands are removed in the same temperature range (140–210 °C), immediately followed by the ammonium cation.

Once the ammonium cation have been decomposed the oxo-molybdate $\{Mo_2O_6\}$ entity is destabilized and starts to decompose by releasing volatiles MoO_3 molecules. The main difference between compound 3 and the other two concerns the decomposition mechanism of these $\{Mo_2O_6\}$ entities. Their decomposition starts at higher temperature (450 °C) as compared to compounds 1 and 2 (340 °C). Then, above these temperature thresholds the mass loss is significantly lower for compound 3 (17 wt%) than for compounds 1 (26 wt%) and 2 (36 wt%). As a result, the TGA analysis of compounds 3 leaves a relatively higher amount of solid residue (22 wt%) while compounds 1 and 2 leave 8 wt % and 0 wt%, respectively. This singularity in thermal properties of compounds 3 can be related to differences in its crystal structure. Indeed, the anion-anion connections occur by lattice water molecules in compound 3 instead of ammonium cations as in compounds 1 and 2. This induces changes in the nature of H bonds and interactions between the binuclear $[Mo_2O_6(C_2O_4)_2]^{4-}$ anions, and subsequently affects the stability of the $\{Mo_2O_6\}$ core. Compound 3 is also the only one where the anion is stabilized by tertiary ammonium counterions. The difference in stability of compounds (1) and (2) is probably due to a difference in crystalline cohesion. In compound (2), the crystalline cohesion of the compound in infinite layers is ensured by Van der Waals interactions whereas in compound (1) this cohesion is by hydrogen bonds. The interactions of the hydrogen bonding type are stronger than the Van der Waals type interactions, which is why (1) is thermally more stable than (2). TGA thus could suggest that the $[Mo_2O_6(C_2O_4)_2]^{4-}$ anion is thermally much more stable when isolated with tertiary ammonium cations.

3.7. Redox properties

The redox properties of compounds (1–3) were studied by cyclic voltammetry (CV) in DMSO with 0.1 M NBu_4PF_6 as supporting electrolyte first. The voltammogram of compound (1) is shown in Fig. 5a.

Almost the same voltammograms were obtained for compounds (2) and (3), which contain the same binuclear anion $[Mo_2O_6(C_2O_4)_2]^{4-}$ core. An irreversible oxidative signal at +0.46 V vs Fc^+/Fc can be observed, which is tentatively attributed to the oxidation of the oxalate ligands on the basis of previous studies of metal oxalate complexes [42] or oxalate ions alone [43]. Two mono-electronic reduction signals can also be seen at −1.95 and −2.21 V vs Fc^+/Fc (−1.51 and −1.77 V respectively vs SCE) which probably correspond to the sequential reduction processes of the Mo^{VI} ions (Mo^{VI}-$Mo^{VI} \rightarrow Mo^V$-Mo^{VI} and Mo^V-$Mo^{VI} \rightarrow Mo^V$-Mo^V). These reduction processes are irreversible, since very weak anodic peaks can be observed in the same potential range in the reverse scan. As compared to previously described Mo^{VI} complexes [44,45], the reductions of the metal centers occur here at significantly lower potentials. Reduction of the $[Mo_2O_3(C_2O_4)_4]^{4-}$ anion is not expected to be favored in aprotic solvents such as DMSO, since it results in an increase of the negative charge of the complex. For this reason, the redox behavior of the complex was also examined in water (Fig. 5b). In the available potential range, only one reduction signal was observed at *c.a.* −0.56 V vs SHE (−0.8 V vs SCE). The observation of a single reduction peak suggests that this time the reduction of the two Mo^{VI} centers occurs simultaneously (Mo^{VI}-$Mo^{VI} \rightarrow Mo^V$-Mo^V). This signal exhibits a −50 mV/pH unit dependency (see Table 4), showing that the transfer of electrons is accompanied by the uptake of protons. On the reverse scan, two anodic peaks can be observed at *c.a.* −0.05 and +0.85 V vs SHE. We note that oxalate ions show an irreversible oxidation signal at 0.1 V vs SHE at pH 4.7 (see Fig. SI5, in Supporting information), so one of these anodic peaks is probably due to oxalate. Unlike previously described monomeric Mo^{VI} catechol complexes [46], $[Mo_2O_3(C_2O_4)_4]^{4-}$ does not show an ideal reversible reductive behavior even at relatively fast scan rates.

4. Conclusion

In summary, from two key precursors, ammonium heptamolybdate tetrahydrate and oxalic acid, three new inorganic-organic hybrids based on dinuclear molybdenum(VI) complexes have been prepared by one-pot strategy and their structures determined by X-ray crystallography. X-ray studies showed that all compounds have the same binuclear anion $[Mo_2O_6(C_2O_4)_2]^{4-}$, in which the molybdenum centers connected by a di-(μ-oxo) bridge are each coordinated by a monochelating oxalate and two oxo ligands. An exhaustive bibliographic synthesis shows that this binuclear anion $[Mo_2O_6(C_2O_4)_2]^{4-}$ represents today the fourth category of the series of binuclear molybdenum oxalate compounds. In order to achieve well-refined and reliable molecular identities, this X-ray diffraction analysis has been coupled with IR and Raman spectroscopic studies. The thermogravimetric analysis shows a good correspondence between theoretical and experimental losses of masses. All the compounds exhibit good thermal stability but the ATG study revealed that the binuclear anion $[Mo_2O_6(C_2O_4)_2]^{4-}$ could thermally be much more stable if isolated with tertiary ammoniums such as the $[HDabco]^+$ cation. The thermal decomposition in the solid state of the $\{Mo_2O_6\}$ core is likely influenced by interactions between $[Mo_2O_6(C_2O_4)_2]^{4-}$ anions in the crystal structure. A singularity has been found for compound 3 since lattice water molecules instead of ammonium cations as in compounds 1 and 2 ensure such interactions. As a result, decomposition of $\{Mo_2O_6\}$ core starts later (450 °C)

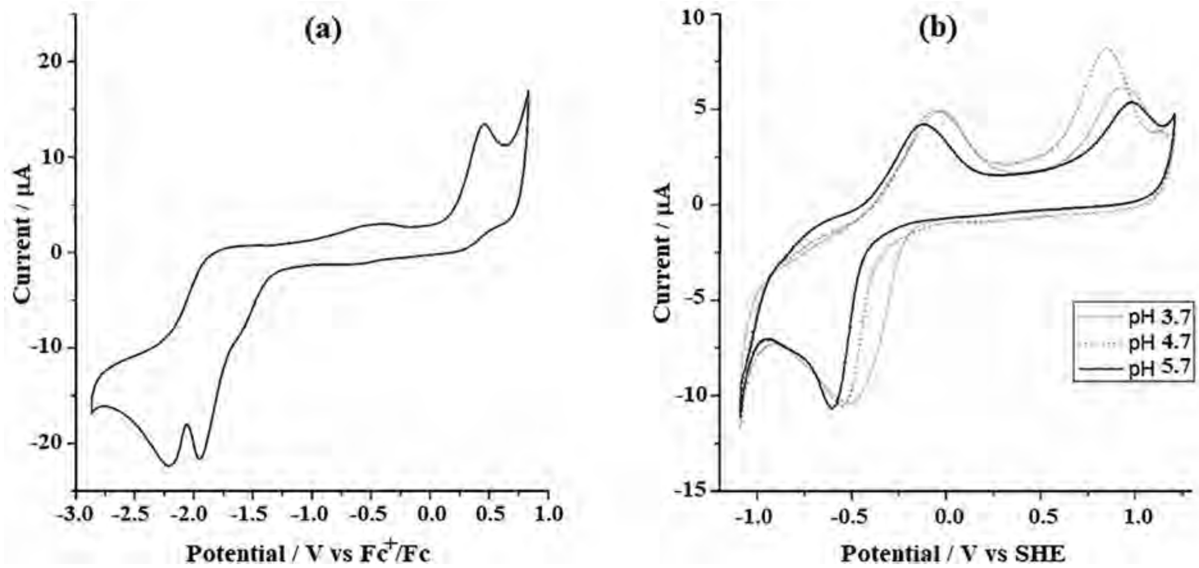

Fig. 5. Cyclic voltammograms of compound (1) in DMSO + 0.1 M nBu_4PF_6 (a) and in H_2O + 0.1 M KCl at different pH values (b). Scan rate 0.1 V s^{-1}.

Table 4
Peak potentials observed for compound (1) in water.

pH	E_{pa}(V)	E_{pc}(V)
3.7	−0.03; +0.93	−0.51
4.7	−0.05; +0.85	−0.56
5.7	−0.12; +0.99	−0.61

compare to other compounds (340 °C), and leaves higher amount of solid residue. On the other hand, these new compounds have very similar redox properties. The cyclic voltammetry shows that the acidity of the medium favors the reduction of the binuclear anion $[Mo_2O_6(C_2O_4)_2]^{4-}$ and reveals that the exchange of $[HDabco]^+$ cation by $[Pr_2NH_2]^+$ or $[^iPr_2NH_2]^+$ cation in stabilization of the binuclear anion $[Mo_2O_6(C_2O_4)_2]^{4-}$ does not affect the electrochemical behavior of the anion. An irreversible oxidative signal centered on the oxalate ligand and two irreversible cathodic signals centered on the metals were observed in aprotic solvent. In water, only one broad and pH-dependent reduction signal was observed and two anodic peaks in the reverse scan. These complexes could play a fundamental role either in the preparation of materials of synthetic or industrial interests, *e.g.* in catalysis or electrochemistry, or in the direct synthesis of antibacterial products. In the further study, we will extend this research to various dinuclear molybdenum(VI) carboxylates.

Acknowledgments

The authors thank the Université Cheikh Anta Diop, Dakar, Sénégal, the Laboratoire de Chimie et Physique des Matériaux (LCPM) de l'Université Assane Seck de Ziguinchor, Sénégal, the CNRS and Université de Strasbourg, France, the CIRIMAT, Université de Toulouse, France and the Faculté des sciences-Aix Marseille Université, France for financial support. All measurements except the TGA were performed in the institutes above quoted. The authors acknowledge also Cédric Charvillat for technical assistance in TGA analyses.

Appendix A. Supplementary material

CCDC-1865458, CCDC-1865459 and CCDC-1865460 contains the supplementary crystallographic data for this paper. These data can be obtained free of charge via http://www.ccdc.cam.ac.uk/deposit@ccdc.cam.ac.uk. Supplementary data to this article can be found online at https://doi.org/10.1016/j.ica.2019.03.037.

References

[1] M. Cindrić, N. Strukan, V. Vrdoljak, Croat. Chem. Acta 72 (1999) 501–509.
[2] M.H. Chisholm, K. Folting, J.C. Huffman, C.C. Kirkpatrick, Inorg. Chem. 23 (1984) 1021–1037.
[3] B.F. Mentzen, H. Sauterean, J. Photochem. 15 (1981) 169–173.
[4] F. Arnaud-Neu, M.J. Schwing-Weill, J. Less-Common Met. 36 (1974) 71–78.
[5] M. Cindrić, N. Strukan, V. Vrdoljak, M. Devčić, Z. Veksli, B. Kamenar, Inorg. Chim. Acta 304 (2000) 260–267.
[6] P. Neves, S. Gago, S.S. Balula, A.D. Lopes, A.A. Valente, L. Cunha-Silva, F.A.A. Paz, M. Pillinger, J. Rocha, C.M. Silva, I.S. Gonc-alves, Inorg. Chem. 50 (2011) 3490–3500.
[7] R. Gupta, H.N. Sheikh, M. Sharma, B.L. Kalsotra, J. Coord. Chem. 63 (2010) 3256–3267.
[8] M. Saleem, M. Sharma, H.N. Sheikh, B.L. Kalsotra, Indian J. Chem. 46A (2007) 1423–1426.
[9] B. Modec, J.V. Brencic, J. Koller, Eur. J. Inorg. Chem. (2004) 1611–1620.
[10] B. Modec, D. Dolenc, J.V. Brencic, J. Koller, J. Zubieta, Eur. J. Inorg. Chem. (2005) 3224–3237.
[11] B. Kamenar, B. Kaitner, N. Strukan, Croat. Chem. Acta. 64 (1991) 329–341.
[12] Q.-L. Chen, H.-B. Chen, Z.-X. Cao, Z.-H. Zhou, Dalton Trans. 42 (2013) 1627–1636.
[13] H.J. Becher, N. Amsoneit, U. Prigge, G. Gatz, Z. Anorg, Allg. Chem. 430 (1977) 255–262.
[14] F.A. Cotton, S.M. Morehouse, Inorg. Chem. 4 (1965) 1377–1381.
[15] M. Cindrić, V. Stilinović, M. Rubčić, G. Medak, D. Šišak Jung, V. Vrdoljak, CrystEngComm 20 (13) (2018) 1889–1898.
[16] B. Sarr, C.A.K. Diop, F. Melin, M. Sidibe, P. Hellwig, F. Michaud, M. Giorgi, F. Maury, F. Senocq, A. Mbaye, Y. Rousseling, J. Mol. Struct. 1170 (2018) 44–50.
[17] G.M. Sheldrick, Acta Cryst. A71 (2015) 3–8.
[18] G.M. Sheldrick, Acta Cryst. C71 (2015) 3–8.
[19] O.V. Dolomanov, L.J. Bourhis, R.J. Gildea, J.A.K. Howard, H. Puschmann, J. Appl. Crystallogr. 42 (2009) 339–341.
[20] H. Cavus, C. Kahruman, I. Yusufoglu, Miner. Met. Mater. Soc. (2012) 785–796.
[21] P.C.H. Mitchell, J. Less-Common Met. 36 (1974) 3–11.
[22] M. Cindrić, N. Strukan, V. Vrdoljak, T. Fuss, G. Giester, B. Kamenar, Inorg. Chim. Acta 309 (2000) 77–81.
[23] B. Modec, D. Dolenc, J. Mol. Struct. 1051 (2013) 354–360.
[24] P. Mialane, L. Lisnard, F. Sécheresse, J. Marrot, G. Costaz, A. Dolbecq, Inorg. Chem. Commun. 5 (2002) 702–705.
[25] K. Routray, L.E. Briand, I.E. Wachs, J. Catal. 256 (2008) 145–153.
[26] C.W. Kee, J. Chem. (2015), https://doi.org/10.1155/2015/439270.
[27] K. Nakamoto, Infrared and Raman Spectra of Inorganic and Coordination Compounds. Part B: Applications in Coordination. Organometallic and Bioinorganic Chemistry, John Wiley & Sons, New York, 2009.
[28] L.I. Berezhinsky, G.I. Dovbeshko, M.P. Lisitsa, G.S. Litvinov, Spectrochim. Acta Part A 54 (1998) 349–358.
[29] M.M.A. Jinnah, M. Umadevi, V. Ramakrishnan, J. Raman Spectrosc. 35 (2004) 956–960.
[30] N.F. Curtis, J. Chem. Soc. A (1968) 1579–1584.
[31] M. Cindrić, V. Vrdoljak, T. Kajfež, P. Novak, A. BrbotŠaranović, N. Strukan, B. Kamenar, Inorg. Chim. Acta 328 (2002) 23–32.
[32] H. Sugimoto, M. Tarumizu, K. Tanaka, H. Miyake, H. Tsukube, Dalton Trans. (2005)

3558–3565.
[33] M. Tašner, B.Z. PrugoveckiSoldin, S. Prugovecki, L. Rukavina, D. Matkovic-Calogovic, Polyhedron 52 (2013) 268–275.
[34] J.M. Coddington, M.J. Taylor, J. Chem. Soc. Dalton Trans. (1990) 41–47.
[35] J. Hanuza, M. Maczka, Vib. Spectrosc. (1995) 417–423.
[36] O.B. Ayodele, Hamisu U. Farouk, Jibril Mohammed, Y. Uemura, W.M.A.W. Daud, J. Taiwan Inst. Chem. Eng. (2014) 1–11.
[37] J. Hanuza, M. Maczka, J.H. van der Maas, Vib. Spectrosc. 8 (1995) 417–423.
[38] K.Y.S. Ng, X. Zhou, E. Gulari, J. Phys. Chem. 89 (1985) 2477–2481.
[39] R. Bhuvaneswari, M. Divya Bharathi, G. Anbalagan, G. Chakkaravarthi, K. Sakthi Murugesan, J. Mol. Struct. 1173 (2018) 188–195.
[40] P.E. Blackburn, M. Hoch, H.L. Johnston, J. Phys. Chem. 62 (1958) 769–773.
[41] L. Brewer, R.H. Lamoreaux, Bull Alloy Phase Diagrams 1 (1980) 85–89.
[42] J.E. Anderson, C.P. Murphy, J. Real, J. Balué, J.C. Bayón, Inorg. Chim. Acta 209 (1993) 151–160.
[43] E. Jacobsen, D.T. Sawyer, J. Electroanal. Chem. 16 (1968) 361–374.
[44] N.K. Ngan, K.M. Lo, C.S.R. Wong, Polyhedron 30 (2011) 2922–2932.
[45] S. Majumder, S. Pasayat, A.K. Panda, S.P. Dash, S. Roy, A. Biswas, M.E. Varma, B.N. Joshi, E. Garribba, C. Kausar, S.K. Patra, W. Kaminsky, A. Crochet, R. Dinda, Inorg. Chem. 56 (2017) 11190–11210.
[46] M.C. Lynn, A.S. Franklin, Inorg. Chem. 19 (1980) 1527–1532.